Piezo-Semiconductor Coupled Model for the Simulation of Zinc Oxide 1–3 Piezo-Composite

Emmanuel Dumons, Louis Pascal Tran-huu-hue, Guylaine Poulin-vittrant

ADVANCED THEORY AND SIMULATIONS
www.advtheorysimul.com

Piezo-Semiconductor Coupled Model for the Simulation of Zinc Oxide 1–3 Piezo-Composite

Emmanuel Dumons, Louis Pascal Tran-Huu-Hue, and Guylaine Poulin-Vittrant*

Semiconducting effects in zinc oxide nanowires-based nanogenerators greatly impact their performances. A coupled model integrating piezoelectric and semiconducting properties is developed with a finite element method to better understand the phenomena involved in this kind of device made with a process including chemical bath deposition of the nanostructures and their polymer encapsulation. Free carriers and surface traps are taken into account to give some keys to explain differences between previous theoretical and experimental works. This model is first validated on a single nanowire with a 10^{16} cm^{-3} n-doping level by comparison with analytical calculations. For this comparison, surface traps are not taken into account as no analytical solution is available considering them. Second, n-doping levels (between 10^{12} and 10^{18} cm^{-3}) and surface traps densities (between 10^{8} and 10^{12} cm^{-2}) lead to variations of the generated piezopotential of two orders of magnitude. The control of these two semiconducting properties is a real challenge for this kind of application. Furthermore, simulation results show that the benefic effect of 1–3 piezo-composite is still present even for a high n-doping level of 10^{18} cm^{-3}.

1. Introduction

In the era of the Internet of Things and the multiplication of devices needing electrical energy to actuate, sense, and communicate, nanogenerators (NGs) have been a promising technology for many years.[1] They have prompted many works to use them as energy micro supply in order to get free from batteries. Until now, most of them have not supplied enough power to reach an industrial scale. Unfortunately, no standard measurement exists but average surface power usually lies between 1 and 100 $\mu W\ cm^{-2}$ depending on the excitation used.[2,3]

As a monocrystalline piezoelectric material, zinc oxide (ZnO) has many advantages such as its availability as a raw material, its biocompatibility, and its compliance with the RoHS directive.[4] However, this material has also semiconducting properties (type II–VI) and most of the time a high n-doping due to the presence of many defects in the crystal,[5,6] responsible for a performance decrease due to free electrons that screen the direct piezoelectric effect.

To target an efficient and inexpensive energy harvester, different solutions have been proposed in the literature, at different stages such as design, manufacturing process, and downstream circuit integration. Regarding the design of the NGs, at the GREMAN laboratory, the choice was made to favor a 1–3 piezo-composite using vertically oriented ZnO piezoelectric nanowires (NWs) embedded in a dielectric polymer matrix. Piezo-composites have been used for a long time and have shown interesting advantages, especially for ultrasonic transducer applications.[7] These structures modulate the mechanical and electrical properties, then leading to an enhanced electromechanical coupling coefficient. To target relatively low production costs of ZnO NWs, the Chemical Bath Deposition (CBD) method offers a simple and industrialisable way to produce ZnO NWs on large substrates.[8] To deliver maximum converted energy to the electric load, various electronic circuits can be connected to the NG output, the basic ones being simple AC-DC converters.[9] When the harvested energy is sufficient, active circuits can be used and increase the efficiency of the full conversion chain.[10,11]

In this work, we focus on the semiconducting properties including the surface traps of ZnO NWs. This paper shows how they modify the direct piezoelectric effect and the generated voltage in a 1–3 piezo-composite NG when a compression force is applied. It is known that CBD leads to a very high doping rate of the ZnO NWs,[12] which theoretically should lead to a quasi-total screening of the piezopotential. Nevertheless, the measurements carried out on NGs incorporating such ZnO NWs[2] reach voltage levels that are in contradiction with the hypothesis of quasi-total screening of the piezopotential. These experimental results suggest that additional phenomena coexist, such as surface traps that could limit the number of free electrons in the NWs core. This could explain why energy harvesting is possible thanks to ZnO NW-based NGs. These surface traps should be added to the existing model of the NG that is itself not trivial, as the NG is

E. Dumons, L. P. Tran-Huu-Hue, G. Poulin-Vittrant
GREMAN UMR 7347 CNRS, INSA Centre Val de Loire
Université de Tours
3 rue de la Chocolaterie, CS 23410, CEDEX, Blois 41034, France
E-mail: emmanuel.dumons@insa-cvl.fr

The ORCID identification number(s) for the author(s) of this article can be found under https://doi.org/10.1002/adts.202300369

DOI: 10.1002/adts.202300369

a multi-layer and composite structure presenting coupled piezoelectric and semiconducting phenomena. In the literature, different types of theoretical studies take into account both phenomena with either analytical calculations or simulations in compression mode. Some of them concern a single NW[13,14] or an NW surrounded by the polymer.[15–17,12] Part of these studies add surface traps to their model and show how this effect is important at the nanoscale.[17,12] Nevertheless, the studies showing the benefits of the 1–3 piezo-composite design[16,18–20] have not yet integrated the semiconducting effect with surface traps.

The first part of this paper describes the principle of the piezoelectric-semiconductor coupled model (PZ-SC model) implemented in COMSOL Multiphysics using the « Solid Mechanics » and « Semiconducting » modules and compares it with a simple analytical case well studied in the literature.[14] In the second part, this paper shows the consequences of the piezoresponse of taking into account semiconductor effects, including those created by surface traps. The aim of this study is to provide a better understanding of the involved phenomena when NGs harvest mechanical energy and to know what are the trends on the generated voltage when NG key parameters are changed. In particular, this study shows that the beneficial effect of the piezo-composite structure 1–3 is maintained, even if the optimum point is modified due to the semiconducting properties.

2. Piezoelectric-Semiconductor Coupled Model

2.1. Assumptions of the Study

This theoretical study is based on Finite Element Method (FEM) using *COMSOL Multiphysics* software (COMSOL Mulitphysics is a trademark of the company COMSOL).

The system for this work is a ZnO NW as a single crystal of wurtzite form (class 6 mm) obtained by CBD on a ZnO nucleation seed layer with a Zn polarity.[21] The NW shape is supposed cylindrical with an axis of revolution coinciding with the *c*-axis of the crystal. The NWs have a radius R of 40 nm and a height h of 500 nm. These values belong to the measurement ranges obtained after the NWs were manufactured on Au/ZnO seed layer at the GREMAN laboratory.[8]

This NW is studied in a compressive mode using static mechanical load along the *c*-axis (considered as the *z*-axis of the frame). It is assumed that the ZnO material remains within the linear elastic domain due to the low mechanical constraints applied to the system.

This NW is considered either alone and electrically isolated, or placed in a polymer matrix all electrically isolated or subjected to periodic conditions simulating the presence of other NWs.

In this study, the semiconductor properties of the ZnO material are added to its piezoelectric properties thanks to a multiphysics coupling not directly provided by the software.

Based on the ANSI/IEEE standard 176–1987,[22] the constitutive equations of a linear piezoelectric system (neglecting thermal effects) link two extensive variables (S_{kl}: strain component and D_{i}: electric displacement field component) and two intensive variables (T_{ij}: stress component and E_{k}: electric field component).

Using the independent variables (S_{kl}, E_{k}) with $i, j, k, l = 1, 2, 3$:

$$T_{ij} = c^{E}_{ijkl}\, S_{kl} - e_{kij} E_k \tag{1}$$

$$D_i = e_{ikl}\, S_{kl} + \epsilon^{S}_{ik} E_k \tag{2}$$

where c^{E}_{ijkl} is an elastic stiffness component at the constant electric field, e_{ijk} a piezoelectric "e" component, and $\epsilon^{S}_{\mathrm{ij}}$ a permittivity component at constant strain.

The h/R aspect ratio of the ZnO NW is sufficiently high to simplify the 3D study into a 1D study along *z*-axis.

Then the constitutive equations of piezoelectricity (in contracted Voigt notation) Equations (3) and (4) and semiconductors Equation (5) are as follows:

$$T_3 = c^{E}_{33}\, S_3 - e_{33} E_3 \tag{3}$$

$$D_3 = e_{33}\, S_3 + \epsilon^{S}_{33} E_3 \tag{4}$$

$$j_{n,3} = nq\mu_{n,33} E_3 + qD_{n,33} \frac{\partial n}{\partial z} \tag{5}$$

where $j_{\mathrm{n},3}$ is the electron current density *z*-component, n the electron density, q the elementary charge, $\mu_{\mathrm{n},33}$ the electron mobility *zz*-component and $D_{\mathrm{n},33}$ the electron diffusion coefficient *zz*-component.

These 1D equations are coupled to Newton's law (Equation 6), Gauss's law (Equation 7), and the charge conservation Equation (8):

$$\frac{\partial T_3}{\partial z} = 0 \tag{6}$$

$$\frac{\partial D_3}{\partial z} = q\left(-n + N_D^{+}\right) \tag{7}$$

$$\frac{\partial j_{n,3}}{\partial z} = 0 \tag{8}$$

and solved at static equilibrium (without other force than the compression ones) for n-doped SC (N_D^{+} is the concentration of donors).

2.2. Piezoelectric-Semiconductor Coupling Model

The original coupling model of the « Solid Mechanics » and « Semiconducting » modules of *COMSOL* software has been implemented as shown in **Figure 1**.

The output variables originating from one module are used as input variables for the other module so that the implemented coupling is bidirectional.

This model can be used for any kind of piezoelectric NG made with semiconducting NWs (ZnO, GaN, ...) whatever the manufacturing method. Input parameters such as NW doping level or surface traps density and traps energy level are needed to apply this model.

For the studies without surface traps, this model is close to previous ones[15,23] but when we add surface traps, this model differs from the others[17,24] because the recombination of free electrons assisted by surface traps is modeled without surface charges (see Section 3.2 for more details). In our model, it is also possible to specify the energy level of these traps in the SC gap. This model will also be used in further works for dynamic studies and for different metal contacts (ohmic or Schottky) with electrodes.

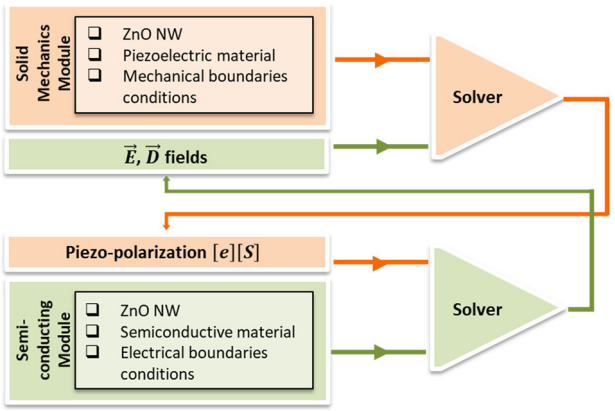

Figure 1. Principle diagram of the PZ-SC coupled model.

Table 1. Boundary conditions for the analytical and numerical comparison.

Boundary conditions	Mechanical	Electrical
NW top face	Compression load of 1 MPa	Isolated
NW lateral face	Free	Isolated
NW bottom face	Compression load of 1 MPa	Isolated

2.3. Analytical and Numerical Comparison

This multiphysics coupling model has been validated by comparing the analytical and numerical results obtained in the case of a single NW subjected to a compression $|T_{ext}| = 1$ MPa at both ends. The schematic of the simulated structure is shown in **Figure 2**a.

The boundary conditions for this study are described in **Table 1**:

Under these conditions, Newton's second law implies that the stress is constant in the NW:

$$T_3 = T_{ext} \tag{9}$$

All donors are assumed to be ionized, so the electronic concentration at equilibrium n_0 is equal to the concentration of donors N_D^+. The electronic concentration can be expressed as

$$n = n_0 + \Delta n \tag{10}$$

with Δn the local variation of the electronic concentration.

Assuming that Δn is very small compared to n_0, analytical solutions for the electronic concentration, the electric field amplitude, and the piezopotential along the NW axis can be calculated.[14] They are shown with the numerical results in **Figure 2**b–d.

These numerical results are in good agreement with the analytical ones. Relative errors of 2%, 11%, and 8% are estimated respectively for the electronic concentration, the electric field amplitude, and the piezopotential.

When considering T_3 constant, it can be demonstrated that there are linear relationships between electric field and strain

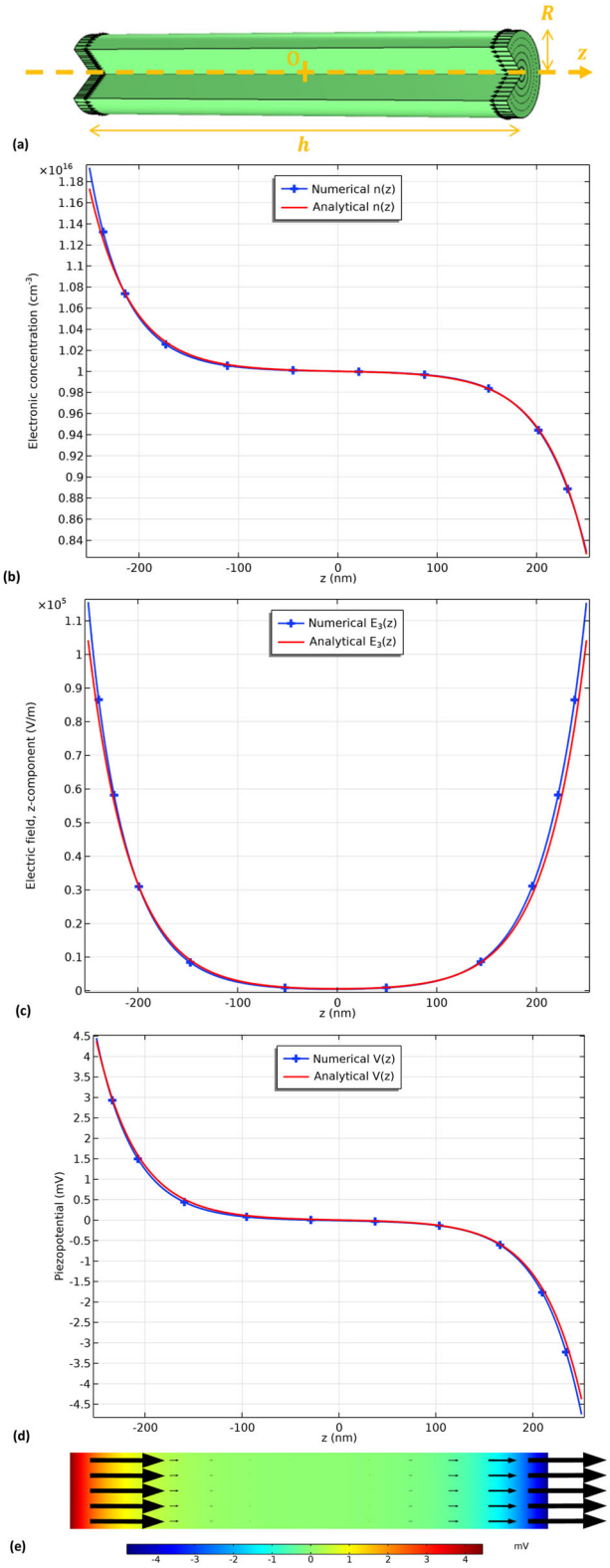

Figure 2. a) Schematic of the simulated structure with the compression loads (black arrows); For a 10^{16} cm^{-3} doping level, evolution along the NW median axis of b) the electronic concentration, c) the electric field amplitude, and d) the piezopotential; e) Piezopotential (colors) and electric field (black arrows) in a median plane.

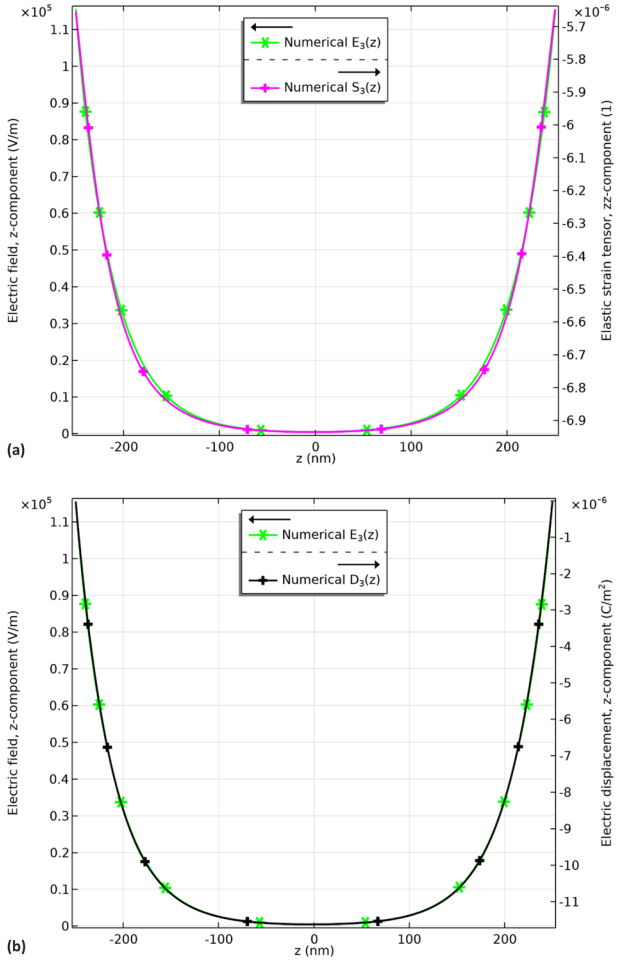

Figure 3. Comparison of the evolutions along the NW median axis of the electric field amplitude and a) the strain zz-component and b) the electric displacement field amplitude.

(Equation 11) and between electric field and electric displacement (Equation 12).

$$E_3 = \frac{1}{e_{33}} \left(c_{33}^E S_3 - T_{\text{ext}} \right) \tag{11}$$

$$E_3 = \frac{1}{\frac{e_{33}}{c_{33}^E} + \epsilon_{33}^S} \left(D_3 - \frac{e_{33}}{c_{33}^E} T_{\text{ext}} \right) \tag{12}$$

This is confirmed by simulation results that give similar evolutions for these pairs of quantities along the *z*-axis, as shown in **Figure 3**a,b.

As a conclusion, this study validates the PZ-SC coupled model in a simple case. However, more complex configurations with electrodes, polymer matrix embedding the NWs, or surface defects of ZnO NWs cannot be solved analytically. In the following, such more realistic configurations will be studied using the new FEM model, to decrease the gap between theoretical studies and experimental values measured on NGs, as observed in the literature.

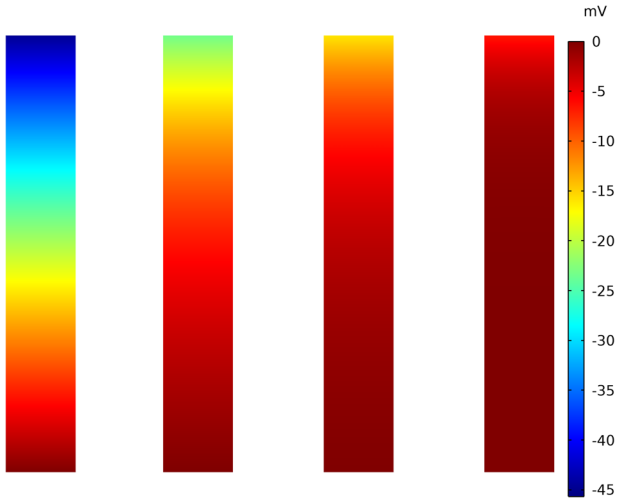

Figure 4. Comparison of piezo-potential distributions in a NW median plane in function of doping level (from left to right: 10^{14}, 5×10^{14}, 10^{15}, and 5×10^{15} cm^{-3}).

Table 2. Boundary conditions for the effect of the doping level.

Boundary conditions	Mechanical	Electrical
NW top face	Compression load of 1 MPa	Isolated
NW lateral face	Free	Isolated
NW bottom face	Roller	Metallic contact (ohmic type)

3. Results and Discussion

Throughout this section, no external electrical circuit is connected to the NW taken alone or embedded with polymer: the calculated voltage is therefore the open circuit voltage. To approximate the experimental electrical conditions,[25] the presence of a metal electrode at the lower end of the NW is simulated using an ohmic « Metal Contact » boundary condition. Mechanically, a uniform compression of 1 MPa is applied to the upper surface of the NW and the lower surface is in a « Roller » condition.

3.1. Effect of the Doping Level on a Single NW

As explained in the introduction, the existence of free electrons in the n-doped ZnO NWs results in the piezopotential screening. **Figure 4** presents the distribution of the piezopotential in a median plane of a compressed NW for several doping levels: the higher the doping level, the higher the screening effect.

The boundary conditions for this study are described in **Table 2**:

The « Roller » boundary condition avoids local normal displacements of the NW bottom face but allows tangent ones to model the influence of a fixed substrate. This kind of boundary condition is more realistic than the « Fixed constraint » one because lateral local displacements for this face are allowed. The bottom electrode is simulated with the « Metallic contact (ohmic type) » boundary condition to have a zero equipotential surface.

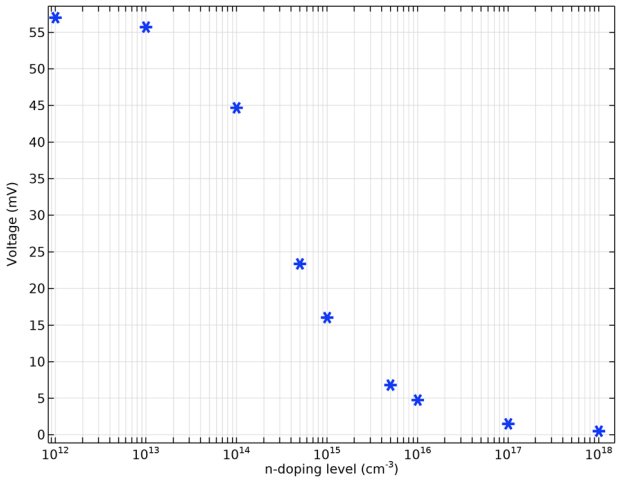

Figure 5. Evolution of the open-circuit voltage between both ends of the NW in function of the n-doping level.

The voltage (positive potential difference between both ends) of the NW is plotted as a function of the doping level in **Figure 5**.

It can be noted that the voltage obtained for a very low doping of 10^{12} cm^{-3} is reduced by a factor of 10 when the doping level reaches 10^{16} cm^{-3} and becomes almost zero for a very high doping level of 10^{18} cm^{-3} that corresponds to the doping level of ZnO NWs obtained by CBD.[12]

To discuss the conversion efficiency of the direct piezoelectric effect in the present work, an effective coefficient g_{33}^{eff} including other effects than piezoelectricity can be quantified.

For non-semiconducting piezoelectric materials, the g_{33} coefficient links the electric field and the stress in open-circuit conditions ($D_3 = 0$ C.m^{-2}) (Equation 13).

$$E_3 = g_{33}\, T_3 \tag{13}$$

For bulk ZnO, $g_{33} = 0.064$ V.m.N^{-1}.[26]

For semiconducting piezoelectric materials, Figure 2b shows that the electric field varies along the length of the NW. By using the mean value of the electric field, the effective coefficient g_{33}^{eff} can be defined by (Equation 14):

$$g_{33}^{\text{eff}} = \frac{\langle E_3 \rangle_z}{T_3} \tag{14}$$

where $\langle E_3 \rangle_z$ is the mean value of E_3 along the z-axis.

To evaluate the effective coefficients g_{33}^{eff} of other works taken from the literature, $\langle E_3 \rangle_z$ is determined thanks to the positive open-circuit voltage ΔV_{oc} and the ZnO NW length h (Equation 15).

$$\langle E_3 \rangle_z = \frac{\Delta V_{\text{oc}}}{h} \tag{15}$$

This estimation method of g_{33}^{eff} is applied to literature data regarding single ZnO NW modeling and the corresponding results are listed in **Table 3**.

The same comparison is done with experimental studies taken from the literature. **Table 4** lists the effective g_{33}^{eff} coefficients calculated using Equations (13) and (14).

Tables 3 and 4 show that there is a wide dispersion in the g_{33}^{eff} values, probably due to different simulation models or experimental configurations. Moreover, all the experimental g_{33}^{eff} values are greater than the theoretical ones and greater than the g_{33} value of bulk ZnO.

That means that numerous effects (surface traps, mechanical behavior of the materials for static, quasi-static, and dynamic modes, mechanical excitation profile, ZnO NWs polarity...) should be added in theoretical models to have a better convergence between theory and experiment. In the next section, we develop the influence of the surface traps in the new PZ-SC model.

3.2. Effect of Surface Traps on a Single NW

One way to explain the experimental values listed in Table 2 is to take into account an important effect for SC materials, that is inherent to surface traps.[34] At the end of the CBD, NWs are dried in the air, which favors the adsorption of oxygen molecules that act as electron acceptor defects as demonstrated in the literature.[35] In the present simulation, electron acceptor traps are added at an energy level of 2.25 eV above the ZnO valence band edge (ZnO bandgap: 3.40 eV). This value corresponds to the electron traps energy level created by superoxide ions O_2^- on ZnO surface after oxygen molecules adsorption.[35] The surface traps create an homogeneous electron current density $\overrightarrow{J_n}$ (Equation 16) through the surface

$$\overrightarrow{J_n}.\ \overrightarrow{n_{\text{ext}}} = -qR_n \tag{16}$$

Table 3. Effective g_{33} values extracted from theoretical studies published in the literature.

Ref.	n-doping [cm^{-3}]	ΔV_{oc} [mV]	h [µm]	$\langle E_3 \rangle_z$ [V.m^{-1}]	Force F_3 [N]	Area $\mathcal{A}$ [m^2]	T_3 [Pa]	g_{33}^{eff} [V.m.N^{-1}]
[13]	1E16	60	2	3E4	442E-9	7.1E-14	6.25E6	0.0048
[27]	1E12	0.15	5	30	10E-6	5E-13	2E7	1.5E-6
[16]	1E16	20	0.6	3.3E4			1E6	0.033
[15]	1E16	42	4	1.05E4	442E-9	7.1E-14	6.25E6	0.0017
[14]	1E16	3	1.2	2.5E3	85E-9	2.6E-14	3.3E6	7.6E-4
[12]	5E17[a)]	730	5	1.5E5			1E6	0.15
[17]	1E16[a)]	66	0.6	1.1E5			1E6	0.12
This work	1E18[a)]	5	0.5	1E4			1E6	0.01

[a)] means surface traps effect taken into account

Table 4. Effective g_{33} values extracted from experimental studies published in the literature.

Ref.	ΔV_{oc} [mV]	h [μm]	$\langle E_3 \rangle_z$ [V.m^{-1}]	Force F_3 [N]	Area $\mathcal{A}$ [m^2]	T_3 [Pa]	g_{33}^{eff} [V.m.N^{-1}]
[28]	270	0.57	4.7E5	3	1E-4	3E4	15.7
[29]	9100	0.5	1.8E7	13	1.2E-4	1.1E5	164
[8]	6800	0.7	9.7E6	3	1E-4	3E4	323
[30]	37 000	10	3.7E6	100	1E-4	1E6	3.7
[31]	>6000	1.1	>5.5E6	6	1E-4	6E4	>92
[32]	4480	2.4	1.9E6	4.9	1E-3	4.9E3	388
[33]	170	2.5 × 2	3.4E4	49	3E-4	1.6E5	0.21

Table 5. Boundary conditions for the effect of surface traps.

Boundary conditions	Mechanical	Electrical
NW top face	Compression load of 1 MPa	Isolated
NW lateral face	Free	Isolated and Trapped assisted surface recombination (with Discrete energy levels)
NW bottom face	Roller	Metallic contact (ohmic type)

that implies a decrease in the total number of free electrons in the ZnO NW.

This current increases with R_n, the recombination rate of these specific traps, which depends on their energy level $\mathcal{E}_t$ and their surface density N_t:

$$R_n = nC_nN_t\left[1 - f_t\left(1 + \frac{1}{g_D}\exp\left(-\frac{\mathcal{E}_{F,n} - \mathcal{E}_t}{k_BT}\right)\right)\right] \quad (17)$$

where C_n is the average capture probability of an electron, f_t the occupancy factor of the traps (in this study, equal to one-half), g_D the degeneracy factor (in this study, equal to one), $\mathcal{E}_{F,n}$ the n-doped Fermi energy level, k_B the Boltzmann's constant and T the temperature.

This model differs from those previously published in the literature[12,17,23,24] that consider surface charge density as a consequence of the surface traps presence.

Due to the nanostructured nature of ZnO, these effects may have greater consequences than for the bulk material because of a higher surface-to-volume ratio.

In the present study, acceptor traps are introduced as a boundary condition on the lateral face of a very highly n-doped NW (doping value of 10^{18} cm^{-3}).

The boundary conditions for this study are described in **Table 5**:

Due to the surface traps, a depletion zone and a bending of the energy levels of the top of the valence band and the bottom of the conduction band appear close to the NW surface as shown in **Figure 6**a,b. This implies a decrease in the total number of free electrons and thus a decrease in the screening effect mentioned in paragraph 3.1.

With a surface traps density $N_t = 10^{12}$ cm^{-2} (order of magnitude for ZnO NWs in literature),[36] the voltage obtained with a high doping level of 10^{18} cm^{-3} is equivalent to the value obtained with a low doping level of 10^{14} cm^{-3} without surface traps. In other words, considering surface traps inside a highly doped NW increases the generated voltage by a factor of 100 as shown in Figure 6c. The surface traps density seems to increase when the NW diameter decreases,[36] which reinforces the interest in nanostructuring. This shows that the existence of surface traps is a possible explanation for the voltage values measured on nanogenerators and published in the literature.

3.3. Effect of a Polymer Encapsulation on a Single NW

In most NGs, ZnO NWs are embedded in a polymer matrix that may be PMMA,[31] PDMS,[37,38] or Parylene C,[8] both to increase the mechanical robustness and prevent internal discharges between adjacent NWs. This design can be seen as a 1–3 piezo-composite, concept introduced by Newnham et al. in 1978,[39] the main difference being the imperfect alignment of ZnO NWs orthogonally to the substrate.[28] Furthermore, to prevent electrical contact between SC ZnO NWs and the top electrode, the NGs manufactured at GREMAN laboratory work in a capacitive mode, thanks to a Parylene C layer deposited on top of the 1–3 piezo-composite structure.[25] When connected to an external circuit, this capacitor can be charged or discharged in function of mechanical excitation. But in the present studies, no external electrical circuit is connected to the NG, and the capacitive layer charges when a compressive load is applied in a quasi-static mode.

To show the effect of the polymer matrix, we consider, in the first step, the polymer coating on the top of the NW, which induces a dielectric capacitive layer. Then, in a second step, the model will include the polymer coating on the top and the lateral side of the NW, which corresponds to the real environment of the NW inside an NG. The Supporting Information presents a similar study performed when the polymer is present on the lateral side of the NW only, which corresponds to a more classical 1–3 piezo-composite. For all these studies, a high doping level of 10^{18} cm^{-3} is considered and 10^{11} cm^{-2} is the highest value for

surface traps density that allows the simulation to converge when the ZnO NW is embedded in the polymer matrix.

3.3.1. Effect of the Polymer Thickness Above the NW

In this part, a dielectric polymer layer is added on top of the NW. A 1 MPa external stress is applied on the top surface of the polymer.

The schematic of the simulated structure is shown in **Figure 7**.

The boundary conditions for this study are described in **Table 6**:

The dependence of the open circuit voltage across the NW with the polymer thickness has been studied for a high n-doping level and different surface traps densities (**Figure 8**).

It can be seen, in Figure 8, that the greater the thickness of the polymer, the greater the voltage. Nevertheless, this effect saturates beyond a given polymer thickness. This saturation appears due to two opposite effects for the electric field in this layer that tend to compensate for each other: the discontinuity of the electric field at the ZnO/polymer interface increases with the polymer thickness but the mean value of this electric field decreases (see the Section 3.3.1 with Figure S1 (Supporting Information) to have more details about this saturation).

Below 50 nm, the polymer thickness has an impact on the voltage amplitude but voltage is not the only important criterion to take into consideration for energy harvesting. The free charges accumulated over the electrodes are equally important[18] as they determine the stored electrical energy.

In literature, experimental works on NGs have been described using various thicknesses of polymer as a capacitive layer but also different polymers: 1 µm of PMMA,[30] 7 µm of PDMS,[38] 300 nm of Parylene C.[8] It could be interesting to study experimentally the influence of the thickness of the same polymer deposited on equivalent ZnO NWs arrays.

3.3.2. Effect of the Polymer Matrix

In this part, the unit cell consists of an NW surrounded on top and laterally by a polymer. For a constant polymer thickness on top of the NW, the effect of the polymer width has been studied on the piezopotential generated by the NW when a 1 MPa pressure is applied on top of the polymer (**Figure 9**a). This study aims to show the effects of the polymer width with or without surface traps on the unit cell. A complementary study is provided when considering the NW only surrounded laterally by a polymer in Section 3.3.2 with Figures S3 and S4 (Supporting Information).

The total width of the unit cell is the sum of twice the polymer width and the NW diameter (see Figure 9a). The NW is topped by a constant thickness of the same polymer (in this study 50 nm). Uniform compression of 1 MPa is applied on the entire top surface of the unit cell. For this study, a high doping level and different surface traps densities are considered.

The boundary conditions for this study are described in **Table 7**:

It can be seen that with the addition of the dielectric polymer layer on top of both the ZnO NW and the laterally embedding polymer, the voltage increases with the polymer width as for the case of the polymer matrix only (see Section 3.3.2 with

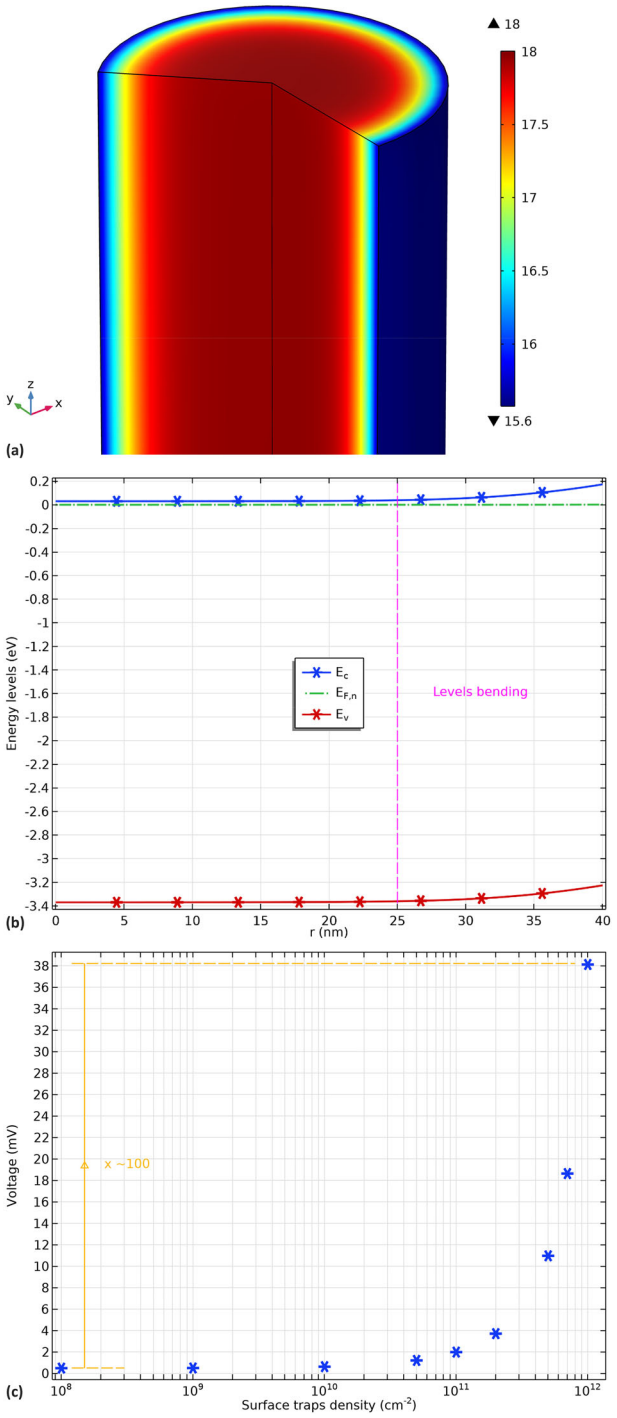

Figure 6. a) Electronic concentration and visualization of the depletion zone, b) Energy levels (in eV) in the function of the radial position, and c) Evolution of the open-circuit voltage between both ends of the NW in the function of the surface traps density (n-doping value 10^{18} cm^{-3}).

Figure 7. Schematic of the simulated structure (green: ZnO NW and cyan: polymer layer) with the compression load (black arrows).

Table 6. Boundary conditions for the effect of the polymer thickness.

Boundary conditions	Mechanical	Electrical
Polymer top face	Compression load of 1 MPa	Zero charge
Polymer lateral face	Free	Zero charge
Polymer bottom/NW top interface	Default (continuity of fields and fluxes)	Insulator interface
NW lateral face	Free	Isolated and Trapped assisted surface recombination (with Discrete energy levels)
NW bottom face	Roller	Metallic contact (ohmic type)

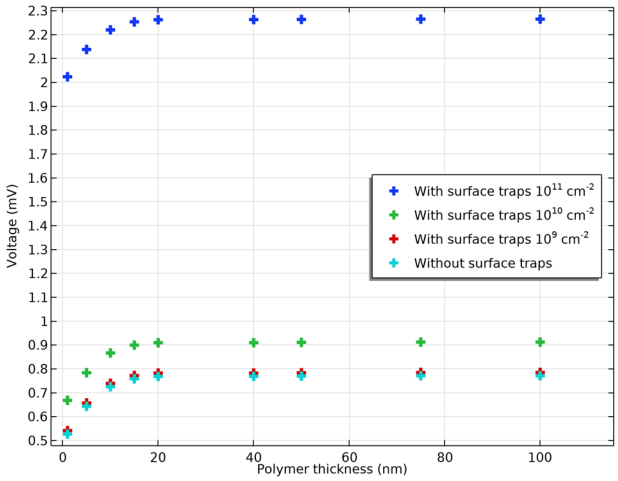

Figure 8. Evolution of the open-circuit voltage between both ends of the NW in function of the polymer thickness (Parylene C) for different cases.

Figure S3a,b, Supporting Information). For the same mechanical reasons,[40] the wider the polymer submitted to the compressive load, the higher the average stress in the NW and so the higher the generated piezo voltage.

Figure 9b shows also that the presence of surface traps does not change the curve shape of the voltage versus the polymer width: there is a voltage gain when the traps are taken into account.

According to this simulation, the voltage increases with the polymer width, but this corresponds to a single NW without taking into account the effect of neighbor NWs. To be more realistic, and predict the behavior of a NW array, the model should take into account the neighbor NWs around a single NW unit cell.

3.4. Effect of the NWs Density on the NG Voltage

In the case of a real NG, the deformation on the lateral face of the polymer is not free. It is, therefore, necessary to take into account the neighboring cells.

Here we propose to study the effect of the NWs surface density over the NG voltage. The underlying purpose of this study is to establish whether the 1–3 piezo-composite structure of the NG is still benefiting from a better mechanical-to-electrical energy conversion even with semiconducting properties.

When only the PZ phenomenon is considered, homogenization of the electromechanical properties of 1–3 piezo-composites was previously achieved by Smith and Auld.[41] However, these calculations do not take into account any SC properties and cannot be directly applied to ZnO. Considering that the homogenized quantities are noted with a top bar, the electrical field is expressed by Equation (18) in open-circuit condition, introducing a homogenized g_{33} coefficient noted $\overline{g_{33}}$.

$$E_3 = \overline{g_{33}}\ T_3 \tag{18}$$

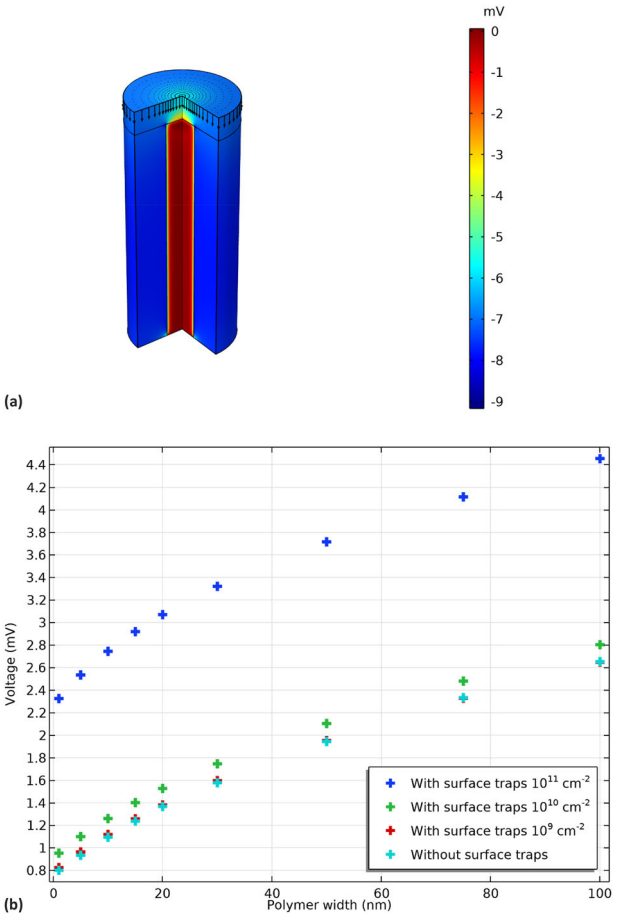

Figure 9. a) Piezopotential for a 75 nm polymer width and a 10^{11} cm^{-2} NW surface traps density (black arrows showing compression), b) Open-circuit voltage between both ends of the NW versus the polymer width for different surface traps density values.

Table 7. Boundary conditions for the effect of the polymer matrix.

Boundary conditions	Mechanical	Electrical
Polymer top face	Compression load of 1 MPa	Zero charge
Polymer lateral face	Free	Zero charge
Polymer bottom/NW top interface	Default (continuity of fields and fluxes)	Insulator interface
NW lateral/Polymer inner lateral interface	Default (continuity of fields and fluxes)	Insulator interface and Trapped assisted surface recombination (with Discrete energy levels)
NW bottom face	Roller	Metallic contact (ohmic type)
Polymer bottom face	Roller	Zero charge

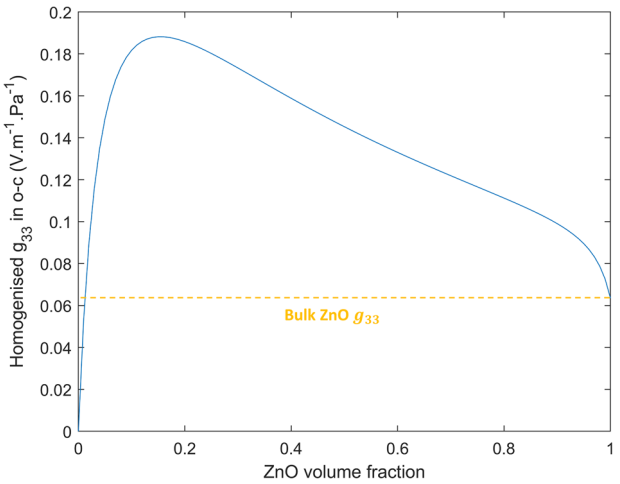

Figure 10. Evolution of the homogenized coefficient $\overline{g_{33}}$ in function of the ZnO volume fraction.

Figure 10 presents the homogenized coefficient g_{33} calculated using (21) for a ZnO volume fraction varying from 0 (absence of ZnO) to 1 (absence of polymer) when SC properties are not taken into account. This curve shows the benefit of the 1–3 piezocomposite structure over a certain range of ZnO volume fraction compared to the bulk material.

Hinchet et al.[16] demonstrated that this benefit exists for nanogenerators with PZ properties only. The purpose here is to verify that there is still an optimum of NWs density when SC effects are added thanks to the new PZ-SC model, even with surface traps.

Using the current PZ-SC model, a 3D study is performed considering an array of NWs embedded in a polymer matrix by using periodic electrical boundary conditions (requiring the use of the Electrostatics Module in addition to the PZ-SC model) and mechanical boundary conditions applied to a unit cell. This parallelepiped unit cell contains a single ZnO NW with a high n-doping level and surface traps. The bottom and top electrodes are both simulated with equipotential surfaces.

The periodic conditions make it possible to simulate the presence of other unit cells next to the one under study. Mechanically, the periodic condition forces both opposite faces to have the same displacement field. Electrically, the periodic condition forces both opposite faces to have the same electrical potential.

The boundary conditions for this study are described in **Table 8**:

Figure 11a shows the new model results representing the generated voltage as a function of the ZnO volume fraction for different values of the n-doping level without surface traps. This new geometry of the unit cell with periodic conditions implies the existence of a maximum voltage at a given optimal ZnO volume fraction.

In Figure 11a, it can be seen that the beneficial effect demonstrated by Smith and Auld is still present even when the SC properties of ZnO are taken into account. It can be seen that the optimum ZnO volume fraction and corresponding NWs density strongly depend on the n-doping level of the NW as plotted in Figure 11b.

Cross-sections of the unit cell with the electrical potential distribution are represented in **Figure 12** for different n-doping levels and different ZnO volume fractions.

It can be seen in Figure 12 that the beneficial effects of the polymer in the 1–3 piezocomposite structure are modulated by the free electrons due to the ZnO SC properties. For high n-doping values and large polymer width, the electrical potential varies a

Table 8. Boundary conditions for the effect of the NWs density.

Boundary conditions	Mechanical	Electrical
Polymer top face	Compression load of 1 MPa	Floating potential
Polymer lateral faces	Periodic condition	Periodic condition
Polymer bottom/NW top interface	Default (continuity of fields and fluxes)	Insulator interface
NW lateral/Polymer inner lateral interface	Default (continuity of fields and fluxes)	Insulator interface and Trapped assisted surface recombination (with Discrete energy levels)
NW bottom face	Roller	Metallic contact (ohmic type)
Polymer bottom face	Roller	Floating potential (same value than the metallic contact)

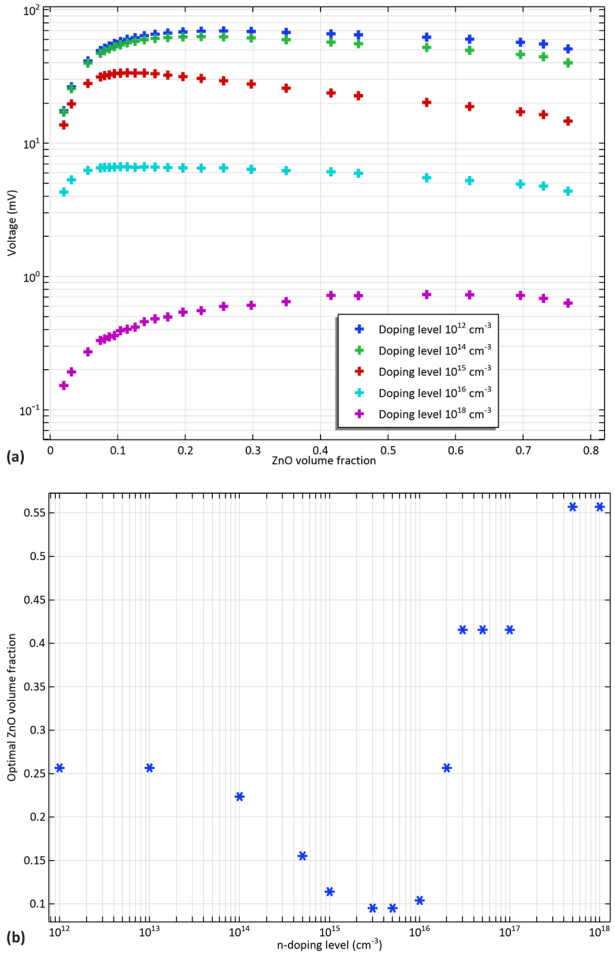

Figure 11. a) Evolution of the open-circuit voltage between both ends of the NW in the function of the ZnO fraction for different n-doping levels without surface traps b) Optimum ZnO volume fraction for different n-doping levels without surface traps.

lot between the ZnO NW top part and the top electrode (see grey arrows in Figure 12). The wider the polymer matrix, the higher the potential variations. These variations in the potential profiles (see Figure S5, Supporting Information) are due in particular to electric field discontinuities. These discontinuities appear in the top part of the ZnO NW where there is a high electronic concentration and at the polymer/ZnO interface where polarization surface charges are accumulated. In this study on the voltage generated by a 1–3 piezocomposite NG in a capacitive mode, there is a trade-off between the mechanical benefit of the polymer matrix and the electrical effects induced by both the polymer matrix and the capacitive layer at the top part of the ZnO NW.

It seems very difficult to validate with experiments the trend for the NWs density depending on n-doping level, as changing this density on the same substrate would also affect their morphology (length, radius) and thus their individual piezoelectric response.

Figure 13a represents the generated voltage as a function of ZnO volume fraction for different values of surface traps density with the same n-doping level of 10^{18} cm^{-3}.

We can see in Figure 13a that the beneficial effect of the 1–3 piezocomposite structure creates an optimum that shifts progressively to a 6% ZnO volume fraction when the surface trap density increases. This optimum is much more visible for high surface traps densities. This seems to be consistent with typical 1–3 piezocomposite characteristics without SC properties (see Figure 10) since the screening effect of free electrons is quite reduced for these surface traps densities.

In the case of a high n-doping level of 10^{18} cm^{-3} and surface traps density of 10^{11} cm^{-2}, as shown on Figure 13a, a maximum voltage ≈5 mV is reached at 6% optimum density. By referring to Section 3.2 and Figure 6c, the generated voltage is multiplied by 20 when the surface traps density increases from 10^{11} to 10^{12} cm^{-2}. Following this trend, the voltage would rise up to 100 mV, which is closer to experimental values (see Table 4).

Figure 13a shows that the NWs surface traps density is an important parameter that modulates the value of the piezopotential but also the optimum NWs density. It can be seen in Figure 13b that, in this case, the optimum ZnO volume fraction increases with the surface traps density due to the effect of the depletion zone, and tends to the optimum fraction of a piezoelectric material without SC properties.

These last two results show that aiming the optimum NWs density for an NG fabrication process requires knowing two major SC properties of the ZnO NWs: their n-doping level and surface traps density. These parameters are difficult to measure and could vary significantly from one fabrication to another, even with the same process and materials.

For the NGs manufactured at GREMAN laboratory with Au/ZnO or ITO/ZnO seed layer, the density is about 40 NWs/μm^2 for an average NW radius of 35 nm.[8] These values give a ZnO volume fraction slightly above 15%, which is higher than the optimum value for high doping level and high surface traps given by the simulation.

4. Conclusion

In the present study, a coupling between piezoelectric and semiconducting properties within a FEM simulation was presented to predict the performance of semiconducting and piezoelectric materials such as ZnO or III-nitrides for mechanical energy harvesting applications. We have shown the major effects of these semiconducting phenomena on the voltage generation by ZnO NWs embedded in a Parylene C matrix, under an external pressure corresponding to usual conditions in low-frequency mechanical energy harvesting. We have also studied the influence of surface traps on ZnO NWs lateral surface. Their presence can multiply the generated voltage up to a factor of 100. Maximizing these surface traps densities by decreasing the diameter of the NWs[36] or by controlling the environment of the NWs[35] is a promising idea to improve the NG performance.

The influence of the polymer matrix around the NWs, thus forming a 1–3 piezo-composite structure, implies the existence of an optimum density that depends on the n-doping level and the surface traps density. These two properties are difficult to measure, which makes the optimum density difficult to predict, while this parameter seems strategic for the design of efficient NGs.

Nevertheless, there is still a gap between experimental and simulated voltage values. More precisely, this gap depends on the

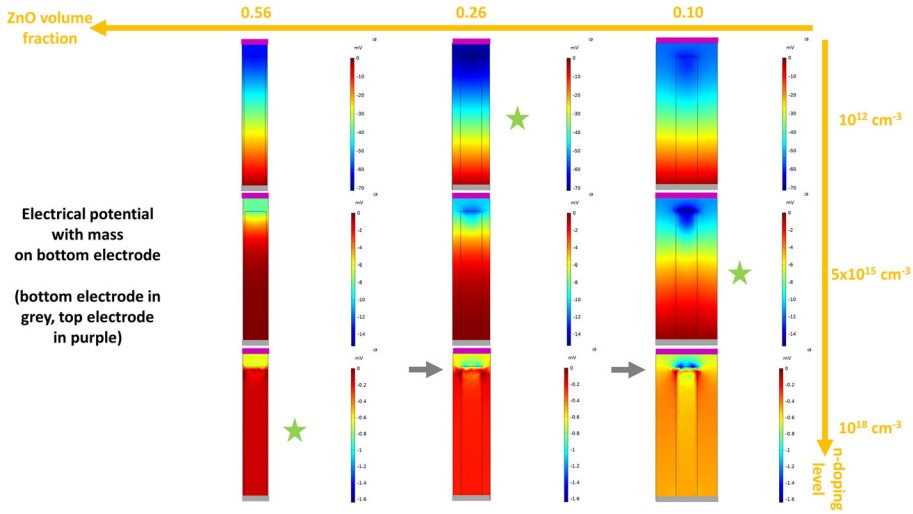

Figure 12. Cross-sections of the unit cell with the electrical potential distribution for different n-doping levels and different ZnO volume fractions (green stars indicate optimal cases).

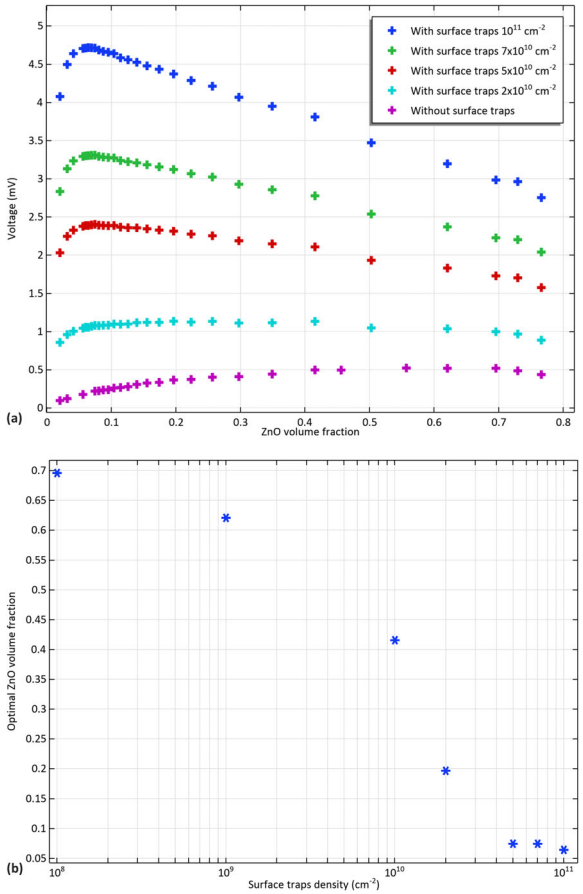

Figure 13. a) Evolution of the open-circuit voltage in function of the ZnO fraction for different surface traps densities and a n-doping level of 10^{18} cm^{-3} b) Optimum ZnO volume fraction for different surface traps densities and a n-doping level of 10^{18} cm^{-3}.

type of experiment performed on NGs. There are large discrepancies between dynamic impact mode[30] that gives a voltage of 37 V and compression in contact mode[33] that gives a voltage of 170 mV for quasi-equivalent stress level. Triboelectricity can also greatly affect the voltage as it is known that this phenomenon occurs much more frequently in impact mode than in contact mode.

Further studies will focus on dynamic mechanical excitation and calculation of the converted energy to explore the optimization trends in that case.

Supporting Information

Supporting Information is available from the Wiley Online Library or from the author.

Acknowledgements

The authors gratefully acknowledge the CNRS Institute for Engineering and Systems Sciences (INSIS), who supports the "Grappillage" project (Gathering of mechanical energy to power sensors for human health monitoring). The authors are also grateful for the support from the Nanomaterials for Energy Applications (GDR NAME, CNRS) research group.

Conflict of Interest

The authors declare no conflict of interest.

Data Availability Statement

The data that support the findings of this study are available from the corresponding author upon reasonable request.

Keywords

1–3 piezo-composite, energy harvesting, nanogenerators, piezo-semiconducting nanowires, surface traps

Received: May 31, 2023
Revised: July 29, 2023
Published online:

[1] X. Zhao, H. Askari, J. Chen, *Joule* **2021**, *5*, 1391.
[2] A. T. Le, M. Ahmadipour, S.-Y. Pung, *J. Alloys Compd.* **2020**, *844*, 156172.
[3] S. Sapkal, B. Kandasubramanian, H. S. Panda, *J. Mater. Sci.: Mater. Electron.* **2022**, *33*, 26633.
[4] Directive 2011/65/EU of the European Parliament and of the Council of 8 June 2011 on the restriction of the use of certain hazardous substances in electrical and electronic equipment (recast) Text with EEA relevance, http://data.europa.eu/eli/dir/2011/65/oj/eng (accessed: June **2011**)
[5] Ü. Özgür, Ya. I. Alivov, C. Liu, A. Teke, M. A. Reshchikov, S. Doğan, V. Avrutin, S.-J. Cho, H. Morkoç, *J. Appl. Phys.* **2005**, *98*, 041301,
[6] C. Klingshirn, *ChemPhysChem* **2007**, *8*, 782.
[7] F. Levassort, J. Holc, E. Ringgaard, T. Bove, M. Kosec, M. Lethiecq, *J. Electroceramics* **2007**, *19*, 127.
[8] T. Slimani Tlemcani, C. Justeau, K. Nadaud, D. Alquier, G. Poulin-Vittrant, *Nanomaterials* **2021**, *11*, 1433.
[9] K. Nadaud, G. Poulin-Vittrant, D. Alquier, *Sens. Actuators, A* **2021**, *330*, 112901.
[10] E. Lefeuvre, G. Sebald, D. Guyomar, M. Lallart, C. Richard, *J. Electroceramics* **2009**, *22*, 171.
[11] T. S. van den Heever, W. J. Perold, *Smart Mater. Struct.* **2013**, *22*, 105029.
[12] A. J. Lopez Garcia, M. Mouis, V. Consonni, G. Ardila, *Nanomaterials* **2021**, *11*, 941.
[13] R. Araneo, G. Lovat, P. Burghignoli, C. Falconi, *Adv. Mater.* **2012**, *24*, 4719.
[14] C. Zhang, X. Wang, W. Chen, J. Yang, *Smart Mater. Struct.* **2017**, *26*, 025030.
[15] G. Romano, G. Mantini, A. Di Carlo, A. D'Amico, C. Falconi, Z. Wang, *Nanotechnology* **2011**, *22*, 465401.
[16] R. Hinchet, S. Lee, G. Ardila, L. Montès, M. Mouis, Z. L. Wang, *Adv. Funct. Mater.* **2014**, *24*, 971.
[17] R. Tao, M. Mouis, G. Ardila, *Adv. Electron. Mater.* **2018**, *4*, 1700299.
[18] R. Hinchet, S. Lee, G. Ardila, L. Montes, M. Mouis, Z. L. Wang, *J. Energy Power Eng.* **2013**, *7*, 1816.
[19] N. Doumit, G. Poulin-Vittrant, *Adv. Theory Simul.* **2018**, *1*, 1800033.
[20] N. Doumit, G. Poulin-Vittrant, *Adv. Theory Simul.* **2020**, *3*, 2000128.
[21] V. Consonni, A. M. Lord, *Nano Energy* **2021**, *83*, 105789.
[22] *IEEE Trans. Ultrason. Ferroelectr. Freq. Control* **1996**, *43*, 717.
[23] A. J. Lopez Garcia, M. Mouis, T. Jalabert, A. Cresti, G. Ardila, *J. Phys. D: Appl. Phys.* **2023**, *56*, 125301.
[24] A. J. Lopez Garcia, M. Mouis, A. Cresti, R. Tao, G. Ardila, *J. Phys. D: Appl. Phys.* **2022**, *55*, 405502.
[25] A. S. Dahiya, F. Morini, S. Boubenia, K. Nadaud, D. Alquier, G. Poulin-Vittrant, *Adv. Mater. Technol.* **2018**, *3*, 1700249.
[26] D. Royer, E. Dieulesaint, *Elastic Waves in Solids I: Free and Guided Propagation*, Springer-Verlag, Berlin, Heidelberg **1999**.
[27] R. Dauksevicius, R. Gaidys, E. P. O'Reilly, M. Seifikar, *Procedia Eng.* **2015**, *120*, 896.
[28] C. Justeau, T. Slimani Tlemcani, G. Poulin-Vittrant, K. Nadaud, D. Alquier, *Materials* **2019**, *12*, 2511.
[29] A. S. Dahiya, F. Morini, S. Boubenia, C. Justeau, K. Nadaud, K. P. Rajeev, D. Alquier, G. Poulin-Vittrant, *J. Phys.: Conf. Ser.* **2018**, *1052*, 012028.
[30] G. Zhu, A. C. Wang, Y. Liu, Y. Zhou, Z. L. Wang, *Nano Lett.* **2012**, *12*, 3086.
[31] L. Serairi, Y. Leprince-Wang, *Crystals* **2022**, *12*, 1023.
[32] R. S. Kammel, R. S. Sabry, *J. Sci.-Adv. Mater. Dev.* **2019**, *4*, 420.
[33] D.-M. Shin, E. L. Tsege, S. H. Kang, W. Seung, S.-W. Kim, H. K. Kim, S. W. Hong, Y.-H. Hwang, *Nano Energy* **2015**, *12*, 268.
[34] H. Lüth, *Solid Surfaces, Interfaces and Thin Films*, Springer, Berlin Heidelberg, **2010**.
[35] J. A. Röhr, J. Sá, S. J. Konezny, *Commun. Chem.* **2019**, *2*, 52.
[36] A. Soudi, C.-H. Hsu, Y. Gu, *Nano Lett.* **2012**, *12*, 5111.
[37] M. R. Hasan, S.-H. Baek, K. S. Seong, J. H. Kim, I.-K. Park, *ACS Publications* **2015**, *7*, 5768.
[38] C. Opoku, A. S. Dahiya, F. Cayrel, G. Poulin-Vittrant, D. Alquier, N. Camara, *RSC Adv.* **2015**, *5*, 69925.
[39] R. E. Newnham, D. P. Skinner, L. E. Cross, *Mater. Res. Bull.* **1978**, *13*, 525.
[40] X. Zhang, J. Villafuerte, V. Consonni, J.-F. Capsal, P.-J. Cottinet, L. Petit, M.-Q. Le, *Nanomaterials* **2021**, *11*, 1712.
[41] W. A. Smith, B. A. Auld, *IEEE Trans. Ultrason., Ferroelect., Freq. Contr.* **1991**, *38*, 40.